NACA RM L51A17

C1

RESEARCH MEMORANDUM

APPLICATION OF THEODORSEN'S PROPELLER THEORY TO THE CALCULATION OF THE PERFORMANCE OF DUAL-ROTATING PROPELLERS

By Jean Gilman, Jr.

Langley Aeronautical Laboratory
Langley Field, Va.

Declassified August 31, 1954

NATIONAL ADVISORY COMMITTEE
FOR AERONAUTICS

WASHINGTON

March 15, 1951

NACA RM L51A17

NATIONAL ADVISORY COMMITTEE FOR AERONAUTICS

RESEARCH MEMORANDUM

APPLICATION OF THEODORSEN'S PROPELLER THEORY TO THE CALCULATION OF THE PERFORMANCE OF DUAL-ROTATING PROPELLERS

By Jean Gilman, Jr.

SUMMARY

Theodorsen's propeller theory is used to calculate the performance of a dual-rotating propeller having nonideal load distributions. The application of this theory to either performance or design calculations of dual-rotating propellers is found to involve a modification to the value of the mass coefficient, which is shown to be affected by the ratio of the spinner radius to the propeller radius. The effect is very important and, since it has not been considered in previous work on this subject, the required modification and the method of application is explained in the present paper.

By using airfoil data which were obtained from the results of special propeller tests, performance calculations are made for an eight-blade dual-rotating propeller with flight Mach numbers varying from 0.53 to 0.90. The calculated results are compared with experimental results for the same propeller. The calculated and experimental power coefficients are found to be in good agreement over the entire range investigated. At a flight Mach number of 0.53, the calculated and experimental efficiences are also in close agreement. At flight Mach numbers of 0.80 and 0.90, the calculated efficiences are from 3 to 6 percent lower than the experimental values. This discrepancy is believed to be due to inaccuracies in the drag data.

INTRODUCTION

In references 1 to 4 Theodorsen presents the ideal circulation functions for single- and dual-rotating propellers as obtained by a method of electrical analogy. As a further step the ideal circulation functions are integrated to obtain values of the mass coefficient. The mass coefficient is used in developing expressions for computing the

thrust, energy loss, and the efficiency of any propeller having the ideal distribution of circulation. The application of these concepts to propeller design is described in reference 5.

The mass coefficient may be interpreted as the ratio of the mean rearward displacement velocity taken over the entire wake cross section to the rearward displacement velocity on the vortex sheets. The mass coefficient is used directly in determining the interference velocities. In practical applications there is a large difference in the mass coefficients of single- and dual-rotating propellers. In view of the foregoing interpretation of the mass coefficient, there is also a large difference in the interference velocities. Hence, the use of the circulation functions of single-rotating propellers in the calculation of the performance of dual-rotating propellers, as has been done in the past, appears inadequate.

The circulation functions for single-rotating propellers obtained in reference 1 are in good agreement with values previously obtained by Goldstein and Lock, which have been found to be adequate for use in performance calculations involving single-rotating propellers at low flight Mach numbers. Very little, if any, insight has been gained, however, as to the applicability of Theodorsen's concepts to calculating the performance of dual-rotating propellers.

It is the purpose of the present paper to test the applicability of the dual-circulation functions in performance calculations by direct comparison with experimental results. Experimental results of the same propeller for which the calculations are made, an eight-blade NACA 3-(3)(05)-05 dual-rotating propeller, are given in reference 6.

During the course of the present work it was found that the ratio of the spinner radius to the propeller radius has an important effect in evaluating the mass coefficient for dual-rotating propellers. In propeller design, this effect can greatly influence the propeller dimensions. The present paper explains the role of the spinner-propeller radius ratio in determining the mass coefficient, and gives a method of application in the design procedure.

The fact that the tests of reference 6 cover flight speeds well up into the transonic range presents an opportunity to test the applicability to dual rotation of airfoil data recently acquired from the results of special propeller tests (reference 7) in the required Mach number range. At low speeds these data are, in general, very similar to the results obtained from standard two-dimensional wind-tunnel tests of the same airfoils. As the critical speed is approached and exceeded, several differences are found to exist between the two sets of data.

In the present paper comparisons are made between the calculated propeller characteristics and the experimental results at flight Mach numbers varying from 0.53 to 0.90. The airfoil data used for the calculations at the lower Mach number are in the range where only small discrepancies exist between the propeller airfoil data of reference 7 and standard two-dimensional data. The differences in the airfoil data are much more pronounced at the higher flight Mach numbers.

SYMBOLS

B	number of propeller blades
b	chord of propeller-blade element
c_d	section drag coefficient
c_l	section lift coefficient
c_{l_d}	section design lift coefficient
P_c	ideal power coefficient
C_P	power coefficient $\left(P/\rho n^3 D^5\right)$
C_Q	torque coefficient $\left(Q/\rho n^2 D^5\right)$
C_T	thrust coefficient $\left(T/\rho n^2 D^4\right)$
D	diameter of propeller
d	drag of propeller section
h	blade-section maximum thickness
J	advance ratio (V/nD)
$K(x)$	circulation function
l	lift of propeller section
M	Mach number of advance
M_x	section resultant Mach number $\left(M\sqrt{1 + \left(\frac{\pi x}{J}\right)^2}\right)$

n propeller rotational speed, rps

P power

Q torque

R tip radius

r radius to any blade element

T thrust of propeller

V velocity of advance

W resultant velocity at blade section

W_o velocity vector $\left(\sqrt{V^2 + (\pi n D x)^2}\right)$

w rearward displacement velocity of helical vortex surface

$\overline{w}$ ratio of displacement velocity to forward velocity (w/V)

x radial location of blade element (r/R)

x_o spinner radius ratio

α angle of attack, degrees

β blade angle, degrees

γ $\tan^{-1} c_d/c_l$

κ mass coefficient $\left(2\int_0^{1.0} K(x)x\,dx\right)$

κ' effective mass coefficient $\left(2\int_{x_o}^{1.0} K(x)x\,dx\right)$

$\Delta\kappa = \kappa - \kappa'$

ϵ axial energy-loss factor

ϵ' axial energy-loss factor based on κ'

η propeller efficiency $(TV/P$ or $JC_T/C_P)$

ρ mass density of air

σ solidity $(Bb/2\pi r)$

σc_l propeller-element load coefficient

ϕ aerodynamic helix angle

ϕ_o geometric helix angle $\left(\tan^{-1} J/\pi x\right)$

Subscripts:

F front

R rear

0.7R at 0.7 radius

INFLUENCE OF SPINNER-PROPELLER RADIUS RATIO ON THE DESIGN OF DUAL-ROTATING PROPELLERS

Although the application of Theodorsen's propeller theory to the design of dual-rotating propellers is described in reference 5, the influence of the spinner-propeller radius ratio on the mass coefficient is not considered. The necessity for including this ratio as a design parameter arises from the large values of the circulation functions occurring over the inner radii for dual rotation, as contrasted to the very small values which occur in single rotation.

The mass coefficient

$$\kappa = 2\int_0^{1.0} xK(x)dx$$

includes the entire propeller-disc area from $x = 0$ to $x = 1.0$, whereas, in actual practice, some of the inner radii are covered by a spinner. There is no circulation within the spinner area and the spinner surface itself may cause interference effects on the remaining flow field. For cases where this interference effect is small, as in the present case, the mass coefficient can be evaluated as

$$\kappa' = 2\int_{x_o}^{1.0} xK(x)dx \qquad (1)$$

The interference velocity is obtained by solving the equation

$$P_c = 2\kappa\bar{w}(1 + \bar{w})\left(1 + \frac{\epsilon}{\kappa}\bar{w}\right) \tag{2}$$

where P_c is known for the design conditions (reference 5). The proper determination of $\bar{w}$, however, requires a modification of equation (2) to

$$P_c = 2\kappa'\bar{w}(1 + \bar{w})\left(1 + \frac{\epsilon'}{\kappa'}\bar{w}\right) \tag{3}$$

Comparison of equations (2) and (3) shows that, for a given P_c, equation (3) yields a larger value of $\bar{w}$ than does equation (2) because κ' is less than κ. The proper evaluation of the quantity $\bar{w}$ is very important because this quantity is used directly in calculating the element loading coefficients σc_l and the aerodynamic helix angles. A dual-rotating propeller which is designed neglecting the spinner propeller radius ratio will tend to operate with heavier than the desired loadings at the design conditions with a consequent loss in efficiency.

The quantity ϵ'/κ' in equation (3) can be obtained in the manner shown in reference 5 by substituting κ' for κ. For many practical purposes, it should be sufficiently accurate to use either ϵ/κ or κ' for ϵ'/κ' because the influence of this quantity in equation (3) is not unduly large.

The effective mass coefficient κ' can be obtained from

$$\kappa' = \kappa - \Delta\kappa$$

where

$$\Delta\kappa = 2\int_0^{x_o} xK(x)dx$$

Up to $x_o \approx 0.4$ the integrand plots approximately as a straight line against x. This fact allows an analytical solution

$$\Delta\kappa \approx x_o^2 K(x_o) \tag{4}$$

which is sufficiently accurate for applications where x_o does not exceed 0.4.

CALCULATION OF PROPELLER CHARACTERISTICS

For ideal conditions with both propellers absorbing equal power at equal rotational speeds and considering both propellers as being very close together, equations for determining the element loading coefficients of dual-rotating propellers are given in reference 5 as follows:

$$\left(\sigma c_l\right)_F = \frac{J}{\pi x} \frac{(1 + \bar{w})\bar{w} \sin \phi_o}{1 + \frac{1}{4} \kappa \bar{w} \sin^2 \phi_o} K(x) \tag{5}$$

and

$$\left(\sigma c_l\right)_R = \frac{J}{\pi x} \frac{(1 + \bar{w})\bar{w} \sin \phi_o}{1 + \frac{3}{4} \kappa \bar{w} \sin^2 \phi_o} K(x) \tag{6}$$

For the same ideal conditions, the aerodynamic helix angles are determined from

$$\tan \phi_F = \frac{J}{\pi x}\left[1 + \frac{1}{2} \bar{w}\left(1 + \frac{1}{2}\kappa \tan^2 \phi\right)\right] \tag{7}$$

$$\tan \phi_R = \frac{J}{\pi x}\left[1 + \frac{1}{2} \bar{w}\left(1 - \frac{1}{2} \kappa \tan^2 \phi\right)\right] \tag{8}$$

where

$$\tan \phi = \frac{J}{\pi x}\left(1 + \frac{1}{2} \bar{w}\right) \tag{9}$$

As noted in the preceding discussion on the influence of a spinner on the κ function, the κ function in these equations should be replaced by κ'. Values of κ and $K(x)$ as functions of the parameter $\frac{V + w}{nD} = J(1 + \bar{w})$ are given in reference 5. These values for an eight-blade dual-rotating propeller (including κ' for $x_o = 0.36$) are given in figure 1.

When the element loading coefficients and the helix angles have been determined (equations (5) to (8)), the element force coefficients can be calculated, provided the drag-lift ratio is known, from the following equations:

$$\left(\frac{dC_Q}{dx}\right)_F = \frac{\pi}{8} J^2\left(1 + \frac{1}{4}\kappa'\overline{w}_F \sin^2\phi_o\right)^2 (\sigma c_l)_F \frac{\cos \phi_F}{\sin^2\phi_o}\left(\tan \phi_F + \tan \gamma_F\right)x^2 \quad (10)$$

$$\left(\frac{dC_Q}{dx}\right)_R = \frac{\pi}{8} J^2\left(1 + \frac{3}{4}\kappa'\overline{w}_R \sin^2\phi_o\right)^2 (\sigma c_l)_R \frac{\cos \phi_R}{\sin^2\phi_o}\left(\tan \phi_R + \tan \gamma_R\right)x^2 \quad (11)$$

$$\left(\frac{dC_T}{dx}\right)_F = \frac{2}{x}\frac{\left(1 - \tan \phi_F \tan \gamma_F\right)}{\left(\tan \phi_F + \tan \gamma_F\right)}\left(\frac{dC_Q}{dx}\right)_F \quad (12)$$

$$\left(\frac{dC_T}{dx}\right)_R = \frac{2}{x}\frac{\left(1 - \tan \phi_R \tan \gamma_R\right)}{\left(\tan \phi_R + \tan \gamma_R\right)}\left(\frac{dC_Q}{dx}\right)_R \quad (13)$$

The derivation of equations (10) to (13) is given in the appendix. For the ideal conditions,

$$\overline{w}_F = \overline{w}_R = \text{Constant}$$

$$\kappa' = \text{Constant}$$

For nonideal cases, experience has shown that satisfactorily accurate calculation of the characteristics of single-rotating propellers can be achieved by considering the circulation functions to be dependent only on the local value of $\overline{w}$. The same assumption is applied for dual-rotating propellers. Dual rotation, however, involves another complication, namely, the mutual interference between the two propellers. In equations (7) and (8), for example, the aerodynamic helix angles of the front and rear propellers are different and this difference depends on the mass coefficient, which is unknown for nonideal cases.

In the present calculations, for lack of better information, it is assumed that κ' for the ideal and nonideal case is not greatly different. At each station κ' is evaluated for the local value of $\overline{w}$ as though the whole propeller operates at the local value.

Before proceding with the calculations, the propeller geometry, the flight Mach number, and the operating J must be given, and a set of suitable airfoil data must be available. When this information is given, the calculations are made by computing $(\sigma c_l)_F$, $(\sigma c_l)_R$, $\tan \phi_F$, and $\tan \phi_R$ (equations (5) to (8)) at appropriate radial stations for

several values of $\overline{w}$. The solidity σ being known, a value of c_l is obtained for each $\overline{w}$ and the corresponding α is determined from the airfoil data. The value of α for a given c_l depends on the section Mach number which is given by

$$M_x = M\sqrt{1 + \left(\frac{\pi x}{J}\right)^2}$$

When α_F and α_R corresponding to each assumed value of $\overline{w}$ are obtained, compute

$$\left(\beta_F\right)_{\overline{w}} = \left(\phi_F + \alpha_F\right)_{\overline{w}}$$

and

$$\left(\beta_R\right)_{\overline{w}} = \left(\phi_R + \alpha_R\right)_{\overline{w}}$$

These values are plotted against $\overline{w}$; the intersection of these curves with the β_F and β_R given by the propeller geometry gives the operating values of $\overline{w}_F$ and $\overline{w}_R$. The operating values of $\overline{w}_F$ and $\overline{w}_R$ are then used in equations (5) to (8) to compute the operating $\left(\sigma c_l\right)_F$, $\left(\sigma c_l\right)_R$, ϕ_F, and ϕ_R for use in equations (10) to (13) (these quantities may also be determined by plotting the trial values against $\overline{w}$ and reading the values corresponding to the operating $\overline{w}_F$ and $\overline{w}_R$). Since the operating σc_l and σ of each propeller are now known, c_l can be determined and can be used to find the corresponding $\tan \gamma$ from the airfoil data for the appropriate section Mach number.

The power and thrust coefficients are given by

$$C_{P_F} = 2\pi \int_{x_o}^{1.0} \left(\frac{dC_Q}{dx}\right)_F dx \qquad (14)$$

$$C_{P_R} = 2\pi \int_{x_o}^{1.0} \left(\frac{dC_Q}{dx}\right)_R dx \qquad (15)$$

$$C_{T_F} = \int_{x_o}^{1.0} \left(\frac{dC_T}{dx}\right)_F dx \tag{16}$$

$$C_{T_R} = \int_{x_o}^{1.0} \left(\frac{dC_T}{dx}\right)_R dx \tag{17}$$

The efficiency is

$$\eta = \frac{J\left(C_{T_F} + C_{T_R}\right)}{C_{P_F} + C_{P_R}} \tag{18}$$

Reference has already been made to figure 1, which shows the $K(x)$ and κ values as functions of the parameter $J(1 + \bar{w})$. The present calculations, in most cases, involve unusually large values of J with the result that values of $J(1 + \bar{w})$ are beyond the range covered in reference 1 and extrapolation, as indicated in the figure, is necessary.

PROPELLER AND AIRFOIL DATA

Description of Propeller

Blade-form curves for the NACA 3-(3)(05)-05 eight-blade dual-rotating propeller are given in figure 2. NACA 16-series airfoil sections are used throughout. The spinner-propeller radius ratio x_o for the particular configuration tested was 0.36. Details of the test setup are given in reference 6. The propeller was tested at forward Mach numbers varying from about 0.35 to 0.925. Blade-angle settings of the front propellers were varied from 55° to 80°. The rear blade angles were set at slightly smaller values, the object being to have each propeller absorb equal power at peak efficiency.

The NACA 3-(3)(05)-05 propeller incorporates a pitch distribution which makes it suitable for operation at an unusually high value of the advance ratio, about 7.2. The propeller consists essentially of two single-rotating propellers of opposite rotation. The $\frac{(bc_l)}{(bc_l)_{x=0.7}}$ curve of this propeller is shown for comparison with the average curve for an ideal (Theodorsen) dual-rotating propeller with $J = 7.15$ in figure 3. This comparison shows that, in terms of the loading at the 0.7 radius,

the test propeller incorporates higher loadings outboard and lower loadings inboard than does the ideal propeller of Theodorsen.

Airfoil Data

Airfoil data used in the calculations are shown in figures 4 to 9. Figures 4 to 6 show the variation of c_d/c_l (or $\tan \gamma$) as a function of section Mach number with c_l as parameter. Figures 7 to 9 show the variation of α with M_x with c_l as parameter.

Data for these figures were obtained from reference 7. The test program of reference 7 involved the measurement of chordwise pressure distributions on a blade of the NACA 10-(3)(066)-033 propeller under operating conditions. By using the circulation functions for single-rotating propellers to determine the interference velocities, it was possible to calculate the two-dimensional airfoil characteristics. Since the method of measurement gives the lift and the pressure drag only, it is necessary to estimate the friction drag. In the present case a friction drag coefficient of 0.004 was used.

The propeller from which the airfoil data were obtained has the same design lift coefficient as the propeller being investigated. The thickness distribution of the two propellers differs, however, which necessitates cross plotting against thickness ratio to obtain data for the proper thickness ratio.

As previously mentioned, comparisons of airfoil data from the results of the special propeller tests with standard two-dimensional wind-tunnel data show comparatively small differences in the subcritical speed range. Beyond this range the differences are more pronounced. Wind-tunnel data in the supercritical range are subject to largely unknown wind-tunnel-wall effects, and it is believed preferable to use the propeller test data in propeller calculations.

RESULTS AND DISCUSSION

Calculations of the propeller characteristics were made for several blade-angle settings and flight Mach numbers. The calculated total-power coefficients and efficiences are compared with experimental values in figures 10 to 12. Figures 13 to 15 give comparisons of the individual front and rear power coefficients. The blade-angle settings, the flight Mach numbers, and the values of J are indicated in the figures.

The calculated total-power coefficients are in very good agreement with the experimental values (figs. 10 to 12). This good agreement indicates that, on the average, the dual-rotating propeller circulation functions give the interference velocities correctly and that the airfoil data show the relation between c_l, α, and M_x properly. Comparisons of the calculated individual front and rear power coefficients with the experimental values (figs. 13 to 15) show that the calculated values for the front propeller are always higher and the calculated values for the rear propeller are always lower than the experimental values. This discrepancy is believed to be due to an assumption in the derivation of the equations that both propellers operate with their planes of rotation very close together.

Comparisons of calculated and experimental efficiency show good agreement between the two sets of data at $M = 0.53$ (fig. 10), but at the higher Mach numbers ($M = 0.8$ and $M = 0.9$, figs. 11 and 12) the calculated efficiency is from 3 to 6 percent lower than the experimental efficiency. This discrepancy is probably caused by inaccuracies in the drag coefficients used in the calculations. Inaccuracies in the drag data would not appreciably affect the calculation of the power coefficients because the drag vector in the torque direction is very small.

CONCLUSIONS

Theodorsen's propeller theory has been applied to the calculation of the characteristics of a dual-rotating propeller having nonideal load distribution. Calculations of the characteristics involved the use of airfoil-section data obtained from the results of propeller tests. Within the range of the investigation, comparison of the calculated results with experimental results leads to the following conclusions.

1. The calculated and experimental total-power coefficients are in good agreement at flight Mach numbers varying from 0.53 to 0.90.

2. The calculated and experimental efficiencies are in close agreement at a flight Mach number of 0.53. At flight Mach numbers of 0.80 and 0.90, the calculated efficiencies are from 3 to 6 percent lower than the experimental values. The discrepancy is believed to be due to inaccuracies in the drag data.

Langley Aeronautical Laboratory
National Advisory Committee for Aeronautics
Langley Field, Va.

APPENDIX

DERIVATION OF FORMULAS FOR CALCULATION OF FORCE COEFFICIENTS

The element torque is

$$dQ = r \frac{1}{2} \rho W^2 Bb \left(c_l \sin \phi + c_d \cos \phi\right) dr$$

With

$$x = \frac{r}{R}$$

$$\sigma = \frac{Bb}{2\pi r}$$

and

$$\tan \gamma = \frac{c_d}{c_l}$$

$$\frac{dQ}{dx} = \frac{\pi D^3}{8} \rho W^2 \sigma c_l \cos \phi (\tan \phi + \tan \gamma) x^2$$

From reference 5

$$W_F = \frac{V}{\sin \phi_o}\left(1 + \frac{1}{4} \kappa' \overline{w} \sin^2 \phi_o\right)$$

and

$$W_R = \frac{V}{\sin \phi_o}\left(1 + \frac{3}{4} \kappa' \overline{w} \sin^2 \phi_o\right)$$

Inserting these equations for the resultant velocities and dividing by $\rho n^2 D^5$ gives the individual front and rear element torque coefficients

$$\left(\frac{dC_Q}{dx}\right)_F = \frac{\pi}{8} J^2\left(1 + \frac{1}{4}\kappa'_F\bar{w}_F \sin^2\phi_o\right)^2\left(\sigma c_l\right)_F \frac{\cos \phi_F}{\sin^2\phi_o}\left(\tan \phi_F + \tan \gamma_F\right)x^2$$

$$\left(\frac{dC_Q}{dx}\right)_R = \frac{\pi}{8} J^2\left(1 + \frac{3}{4}\kappa'_R\bar{w}_R \sin^2\phi_o\right)^2\left(\sigma c_l\right)_R \frac{\cos \phi_R}{\sin^2\phi_o}\left(\tan \phi_R + \tan \gamma_R\right)x^2$$

The element thrust is given by

$$dT = \frac{1}{2}\rho W^2 Bb\left(c_l \cos \phi - c_d \sin \phi\right)dr$$

Substituting as before and dividing by $\rho n^2 D^4$ gives

$$\left(\frac{dC_T}{dx}\right)_F = \frac{\pi J^2}{4}\left(1 + \frac{1}{4}\kappa'_F\bar{w}_F \sin^2\phi_o\right)^2\left(\sigma c_l\right)_F \frac{\cos \phi_F}{\sin^2\phi_o}\left(1 - \tan \phi_F \tan \gamma_F\right)x$$

$$\left(\frac{dC_T}{dx}\right)_R = \frac{\pi J^2}{4}\left(1 + \frac{3}{4}\kappa'_R\bar{w}_R \sin^2\phi_o\right)^2\left(\sigma c_l\right)_R \frac{\cos \phi_R}{\sin^2\phi_o}\left(1 - \tan \phi_R \tan \gamma_R\right)x$$

It is readily seen that

$$\left(\frac{dC_T}{dx}\right)_F = \frac{2}{x}\frac{\left(1 - \tan \phi_F \tan \gamma_F\right)}{\left(\tan \phi_F + \tan \gamma_F\right)}\left(\frac{dC_Q}{dx}\right)_F$$

and

$$\left(\frac{dC_T}{dx}\right)_R = \frac{2}{x}\frac{\left(1 - \tan \phi_R \tan \gamma_R\right)}{\left(\tan \phi_R + \tan \gamma_R\right)}\left(\frac{dC_Q}{dx}\right)_R$$

REFERENCES

1. Theodorsen, Theodore: The Theory of Propellers. I - Determination of the Circulation Function and the Mass Coefficient for Dual-Rotating Propellers. NACA Rep. 775, 1944.

2. Theodorsen, Theodore: The Theory of Propellers. II - Method for Calculating the Axial Interference Velocity. NACA Rep. 776, 1944.

3. Theodorsen, Theodore: The Theory of Propellers. III - The Slipstream Contraction with Numerical Values for Two-Blade and Four-Blade Propellers. NACA Rep. 777, 1944.

4. Theodorsen, Theodore: The Theory of Propellers. IV - Thrust, Energy, and Efficiency Formulas for Single- and Dual-Rotating Propellers with Ideal Circulation Distribution. NACA Rep. 778, 1944.

5. Crigler, John L.: Application of Theodorsen's Theory to Propeller Design. NACA Rep. 924, 1949.

6. Platt, Robert J., Jr., and Shumaker, Robert A.: Investigation of the NACA 3-(3)(05)-05 Eight-Blade Dual-Rotating Propeller at Forward Mach Numbers to 0.925. NACA RM L50D21, 1950.

7. Maynard, Julian D., and Murphy, Maurice P.: Pressure Distributions on the Blade Sections of the NACA 10-(3)(066)-033 Propeller under Operating Conditions. NACA RM L9L12, 1950.

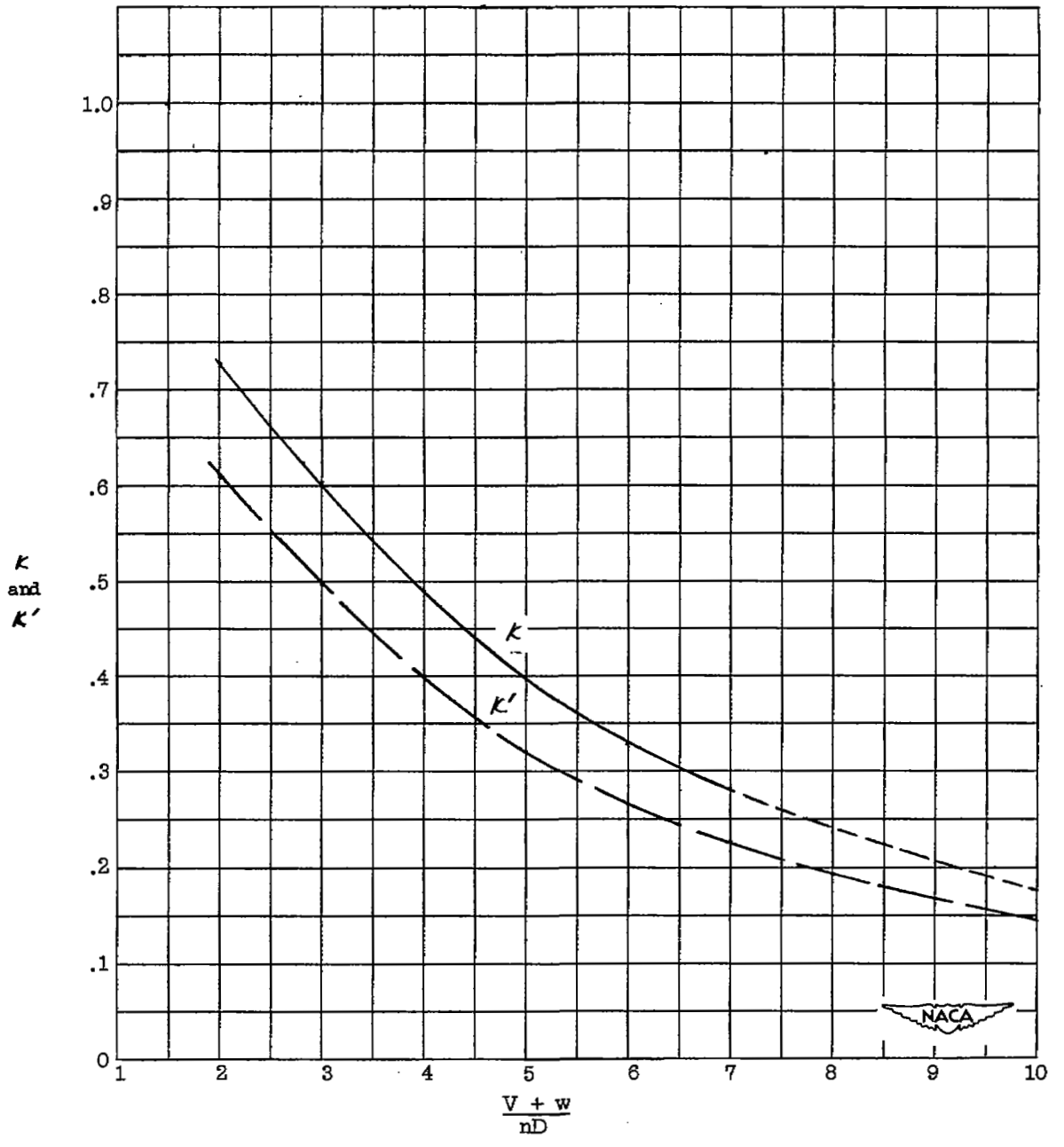

(a) Mass coefficients. x_o for κ' curve is 0.36.

Figure 1.- Mass coefficients and circulation functions for eight-blade dual-rotating propeller. (Short-dash line indicates extrapolation.)

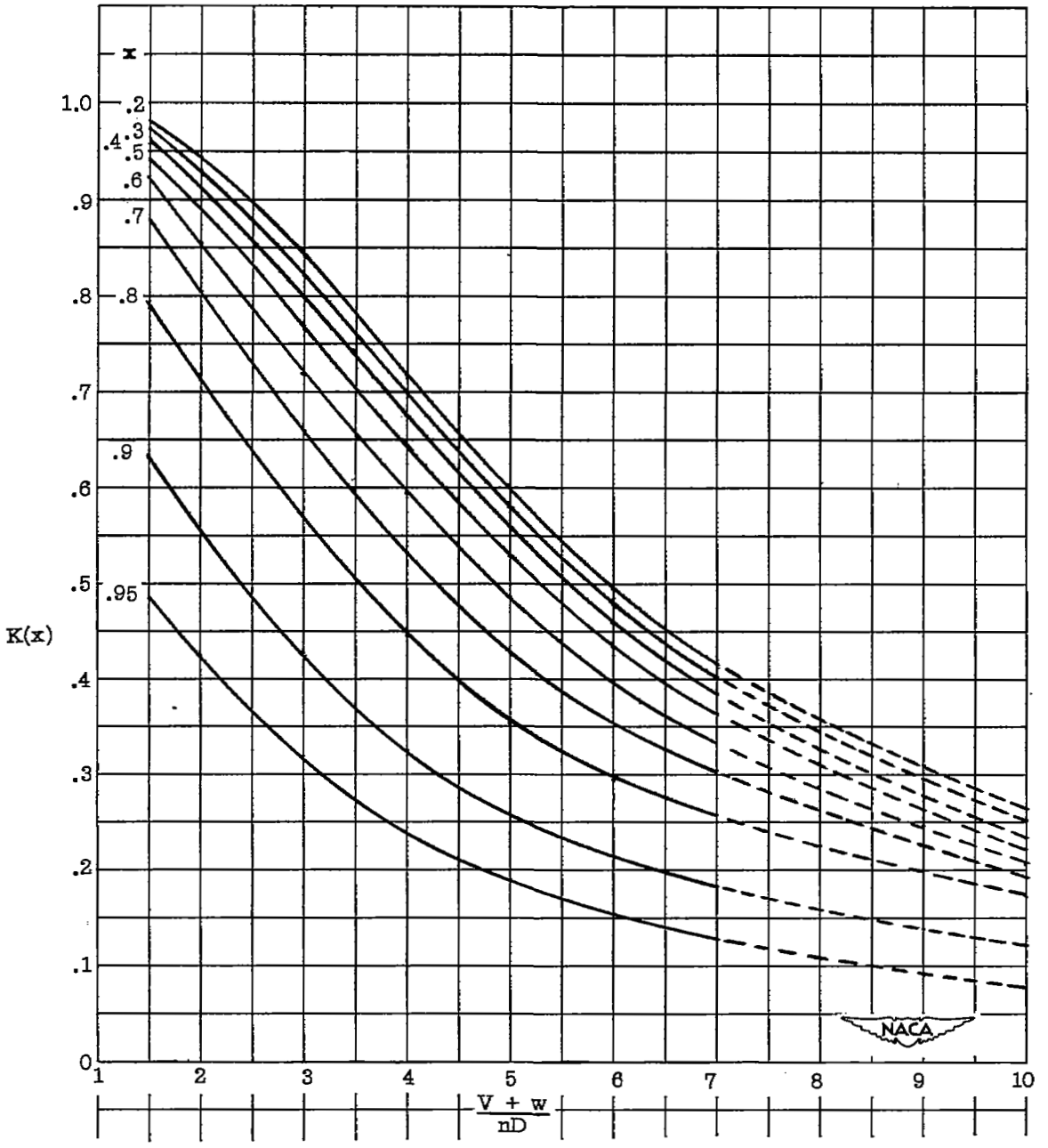

(b) Circulation functions.

Figure 1.- Concluded.

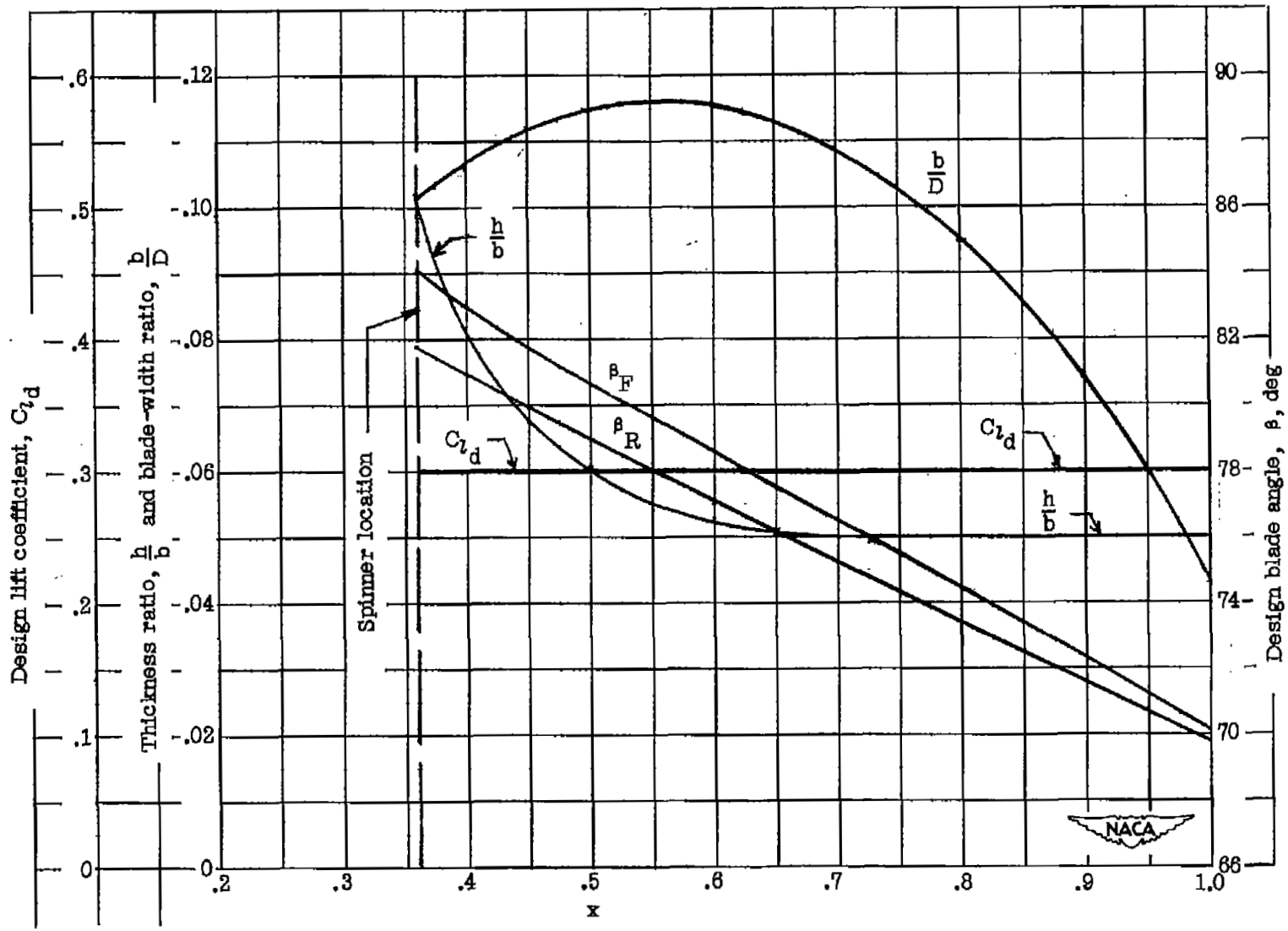

Figure 2.- Blade-form curves for NACA 3-(3)(05)-03 dual-rotating propeller.

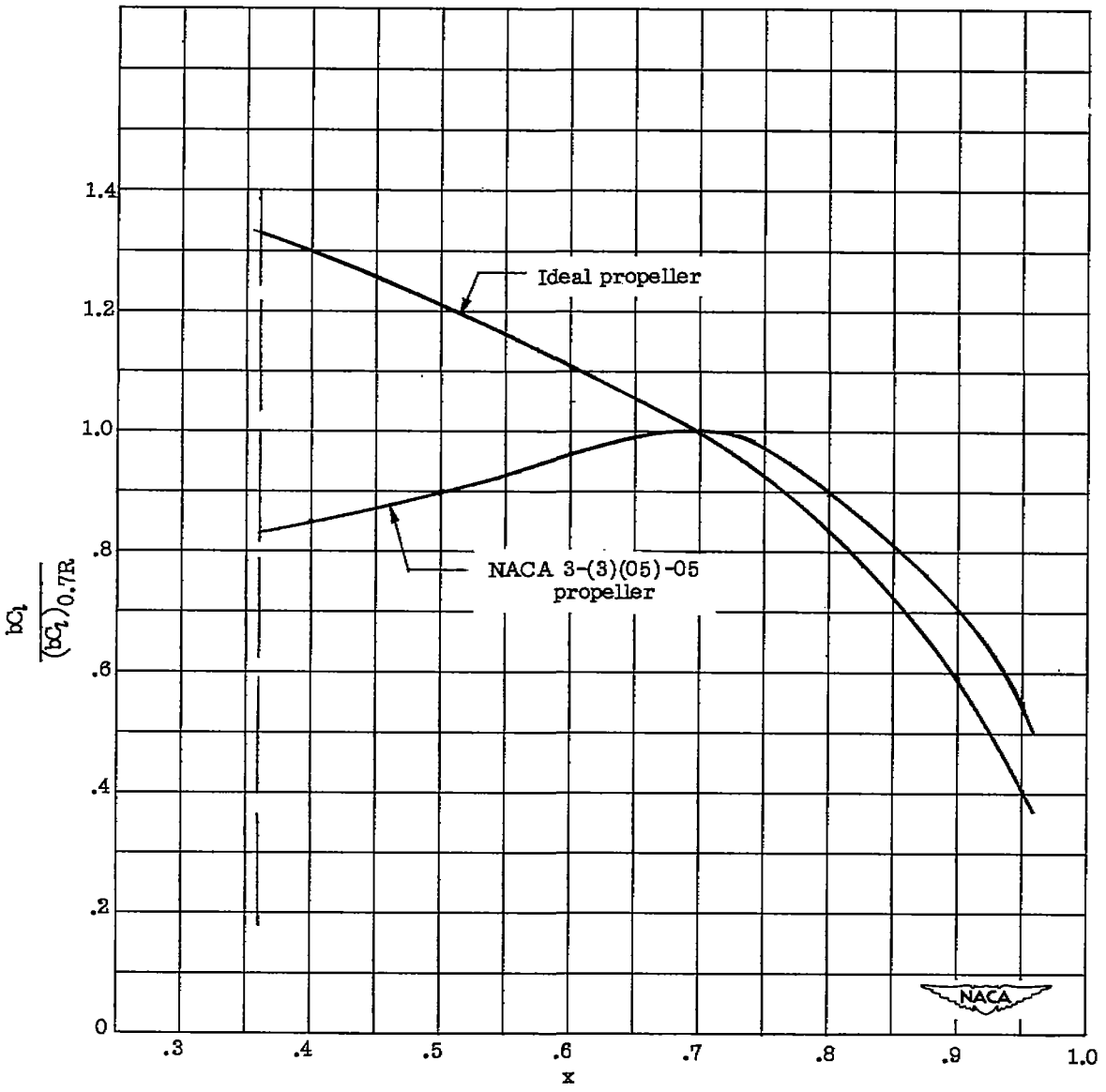

Figure 3.- Comparison of design blade loading of NACA 3-(3)(05)-05 dual-rotating propeller with blade loading of optimum dual-rotating propeller. J, 7.15.

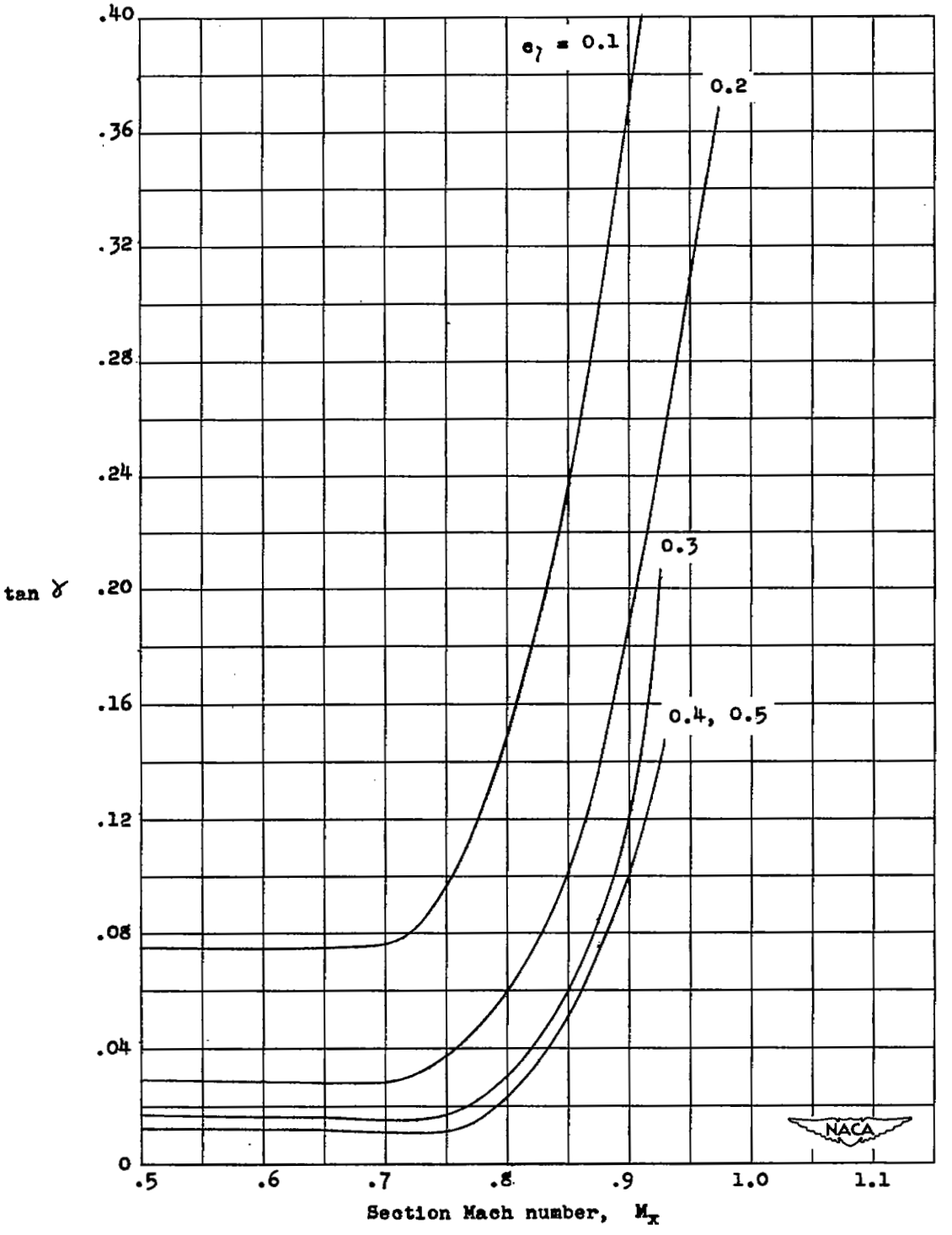

Figure 4.- Drag-lift ratio variation used for station x = 0.45.

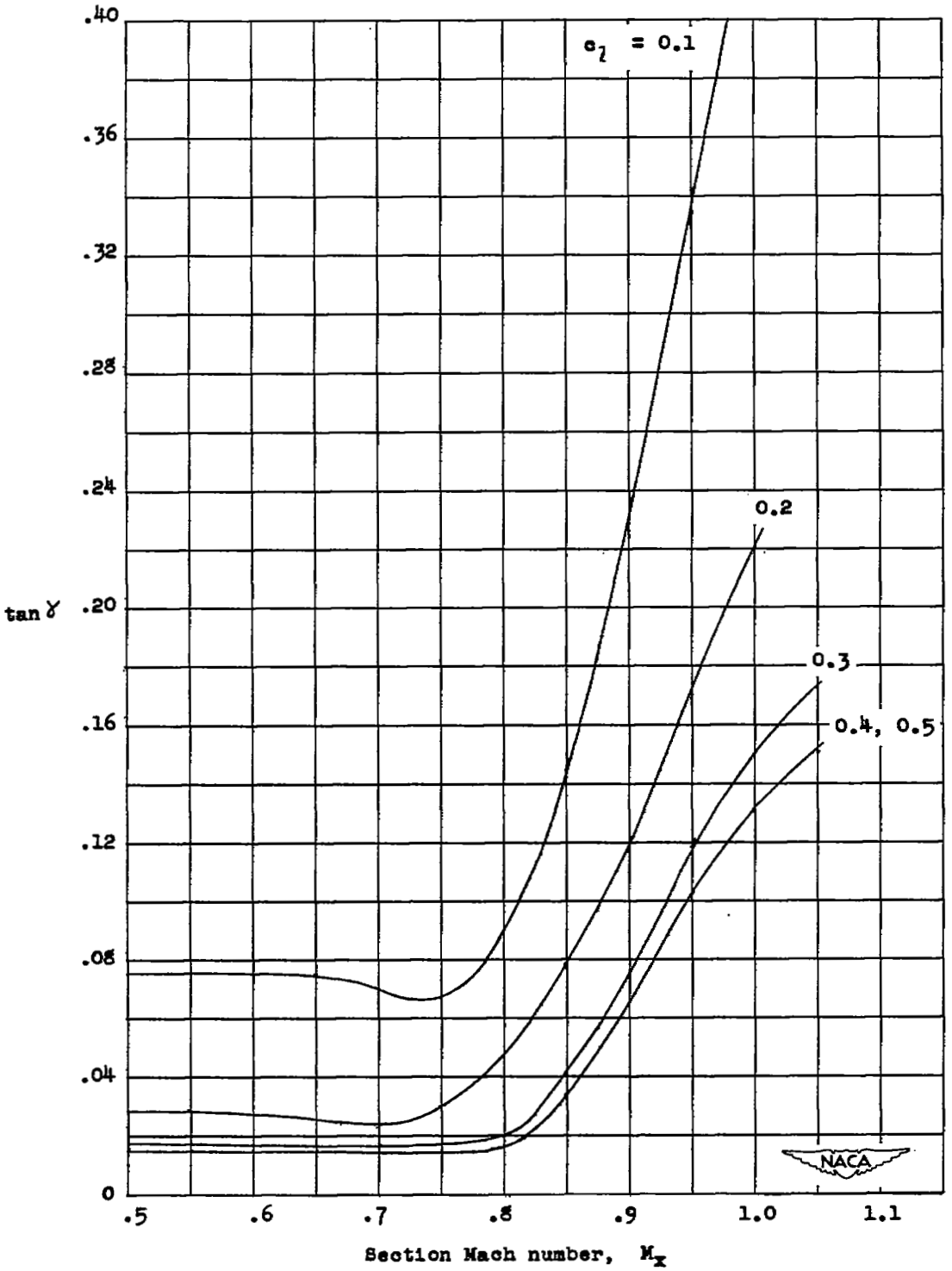

Figure 5.- Drag-lift ratio variation used for station x = 0.60.

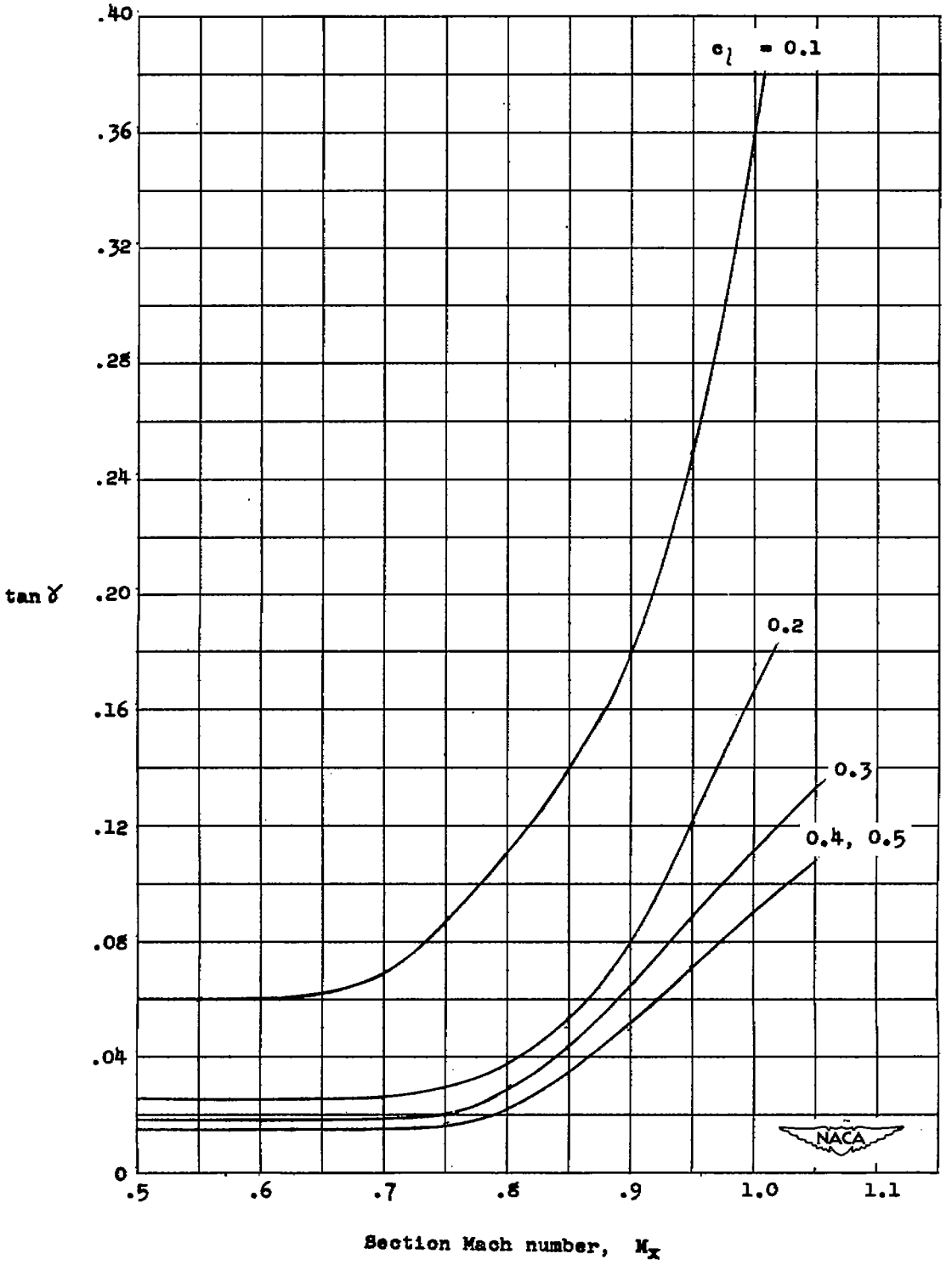

Figure 6.- Drag-lift ratio variation used for stations x = 0.70 to x = 0.95.

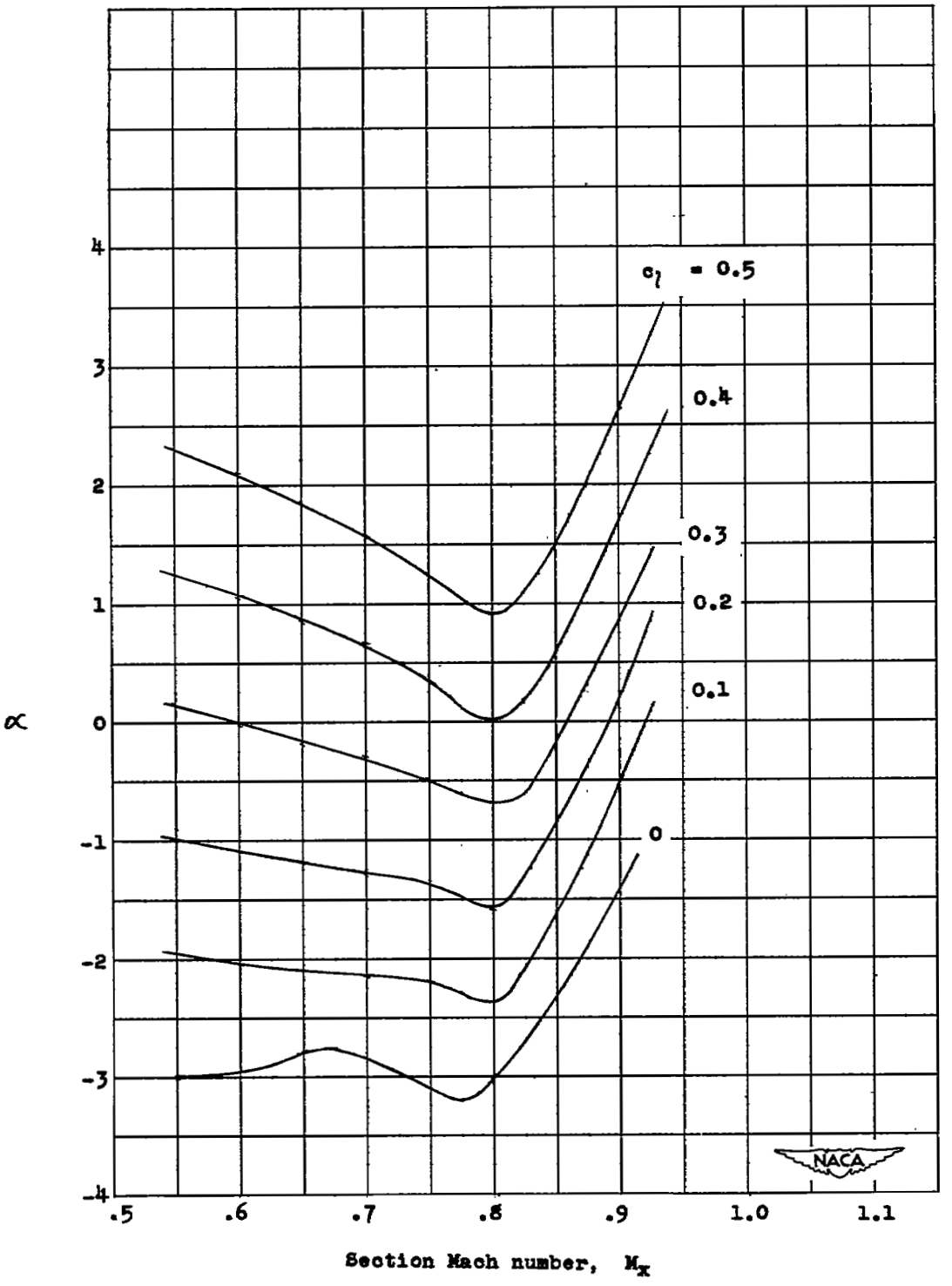

Figure 7.- Angle-of-attack variation used for station x = 0.45.

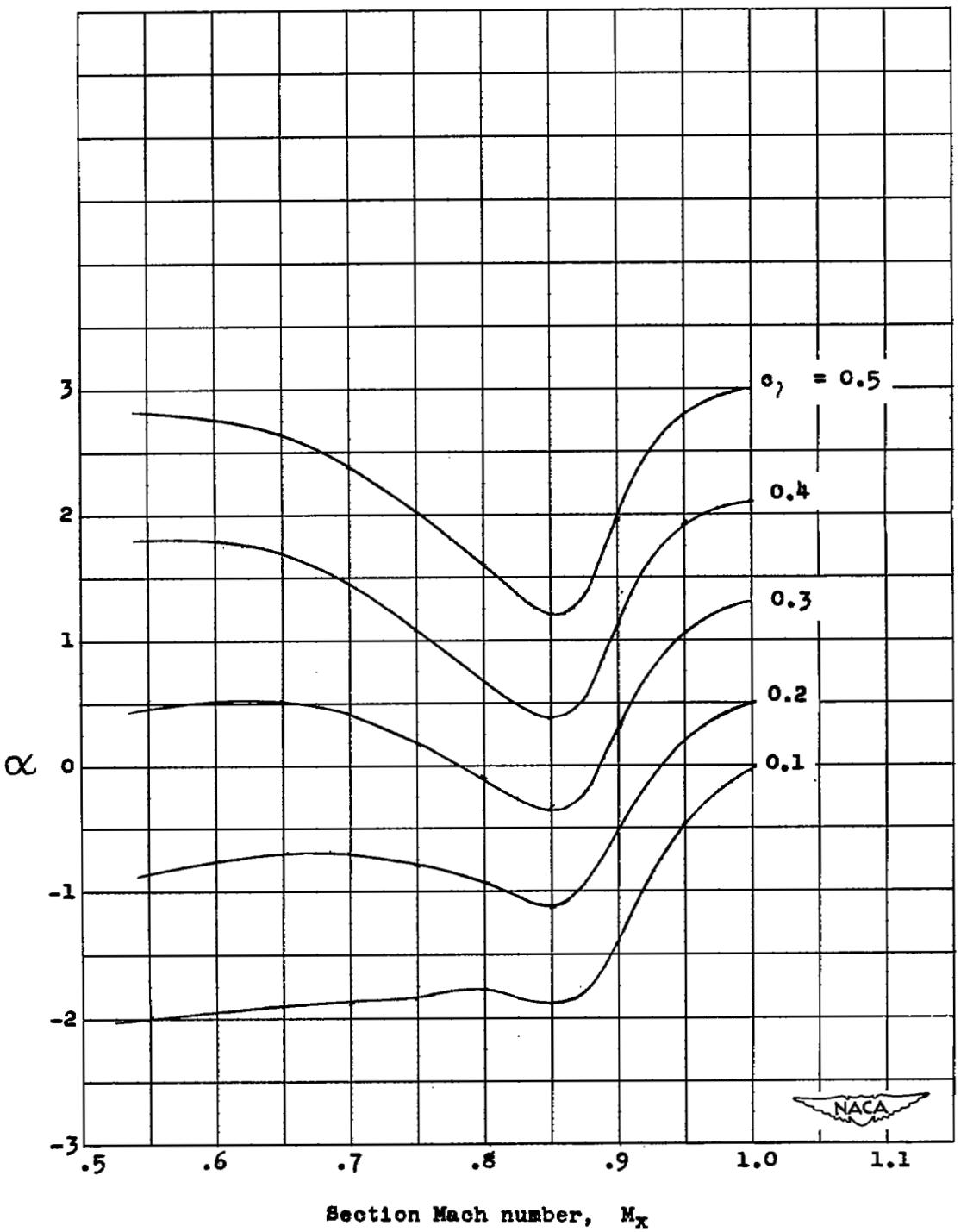

Figure 8.- Angle-of-attack variation used for station x = 0.60.

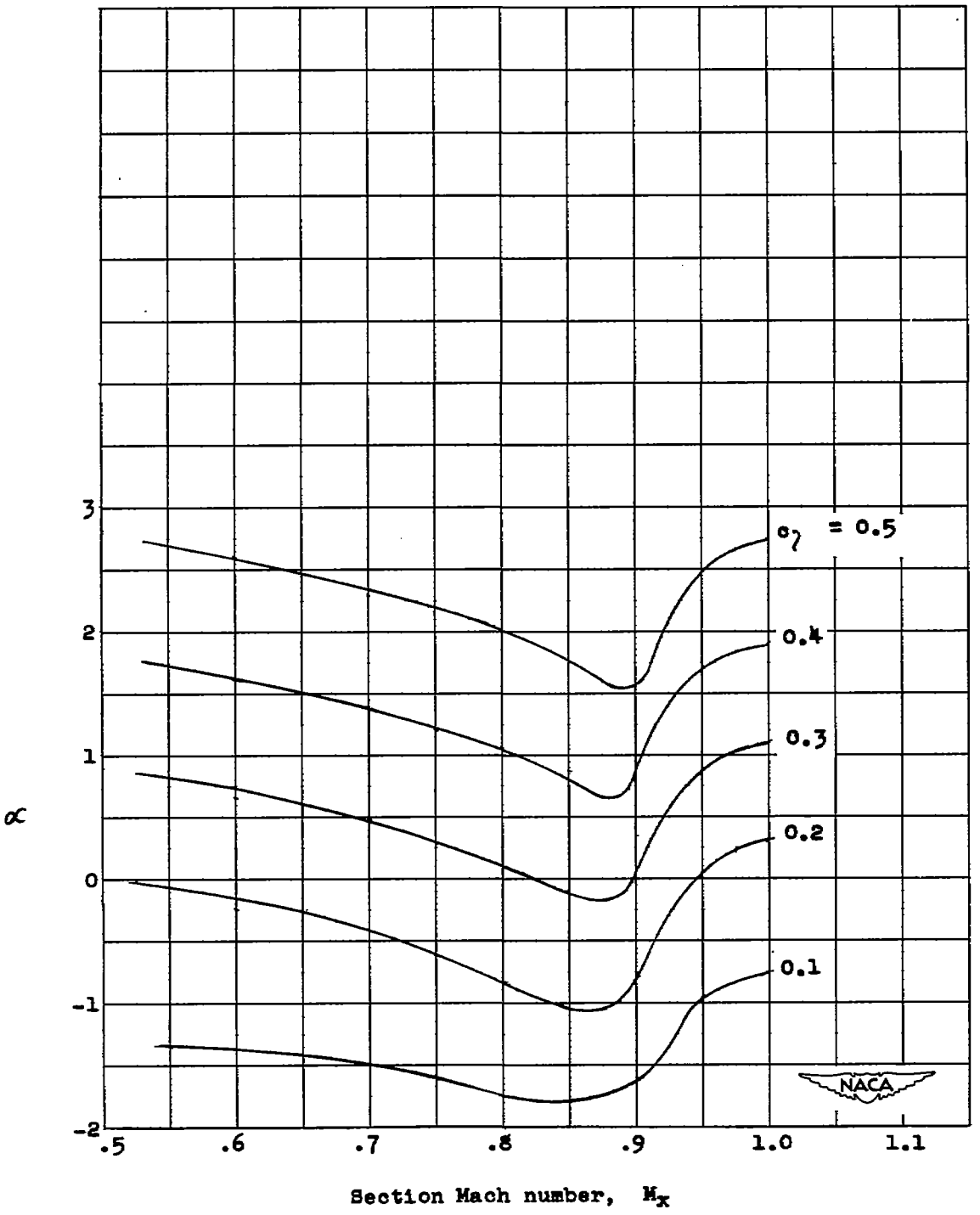

Figure 9.- Angle-of-attack variation used for stations x = 0.70 to x = 0.95.

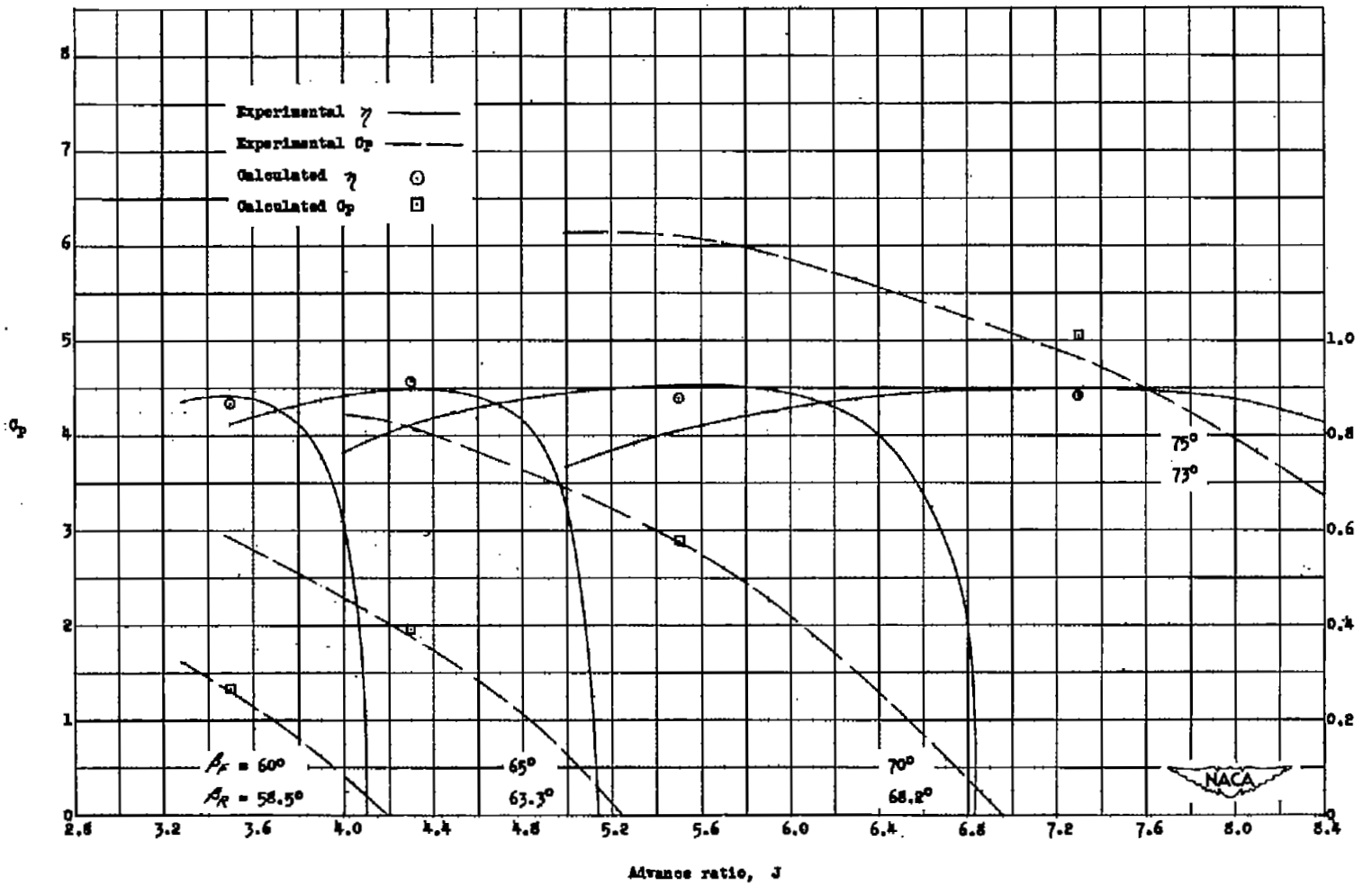

Figure 10.- Comparison of experimental η and C_p with calculated η and C_p. M = 0.53.

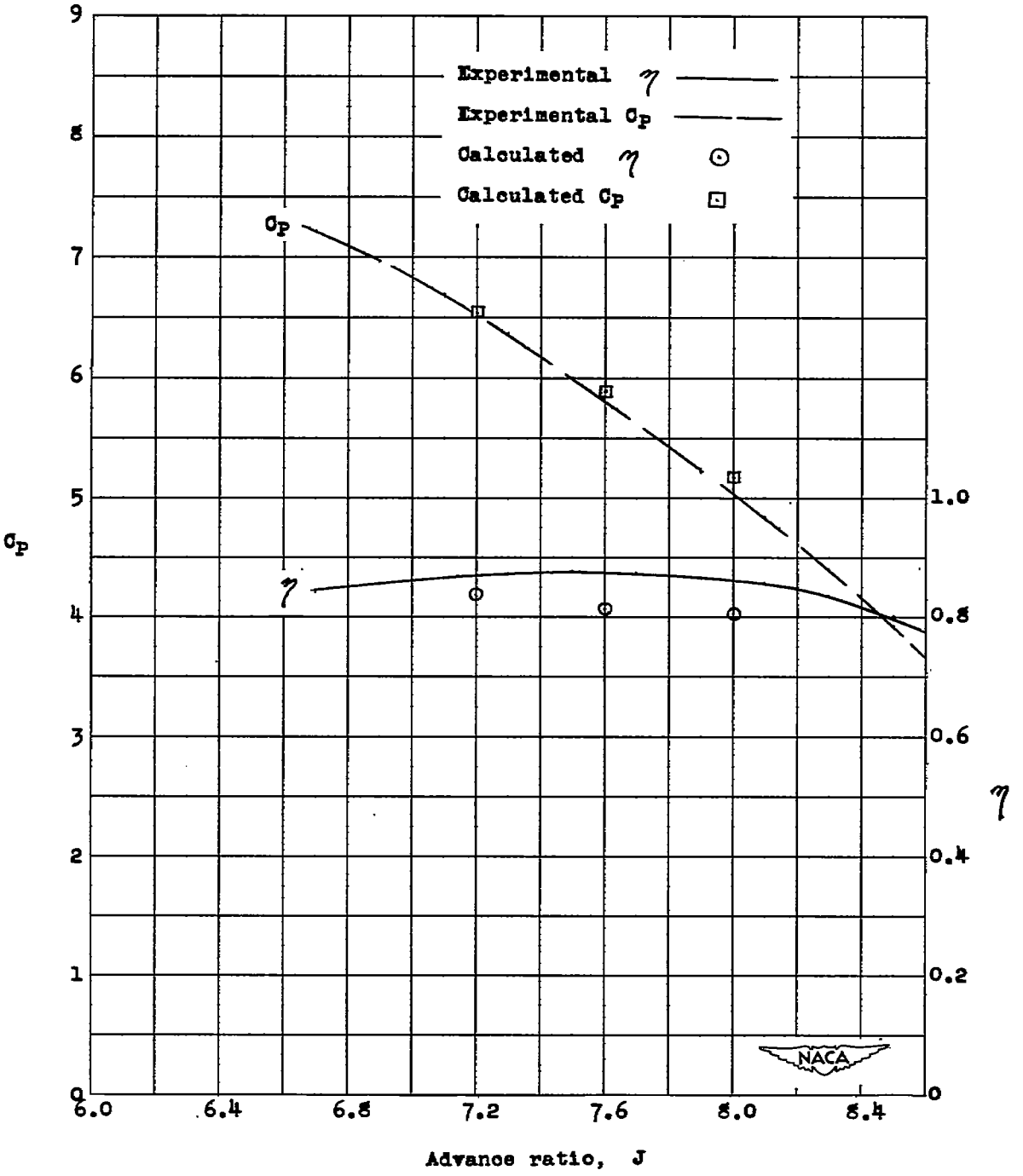

Figure 11.- Comparison of experimental η and C_p with calculated η and C_p. $M = 0.80$; $\beta_F = 75^\circ$; $\beta_R = 73^\circ$.

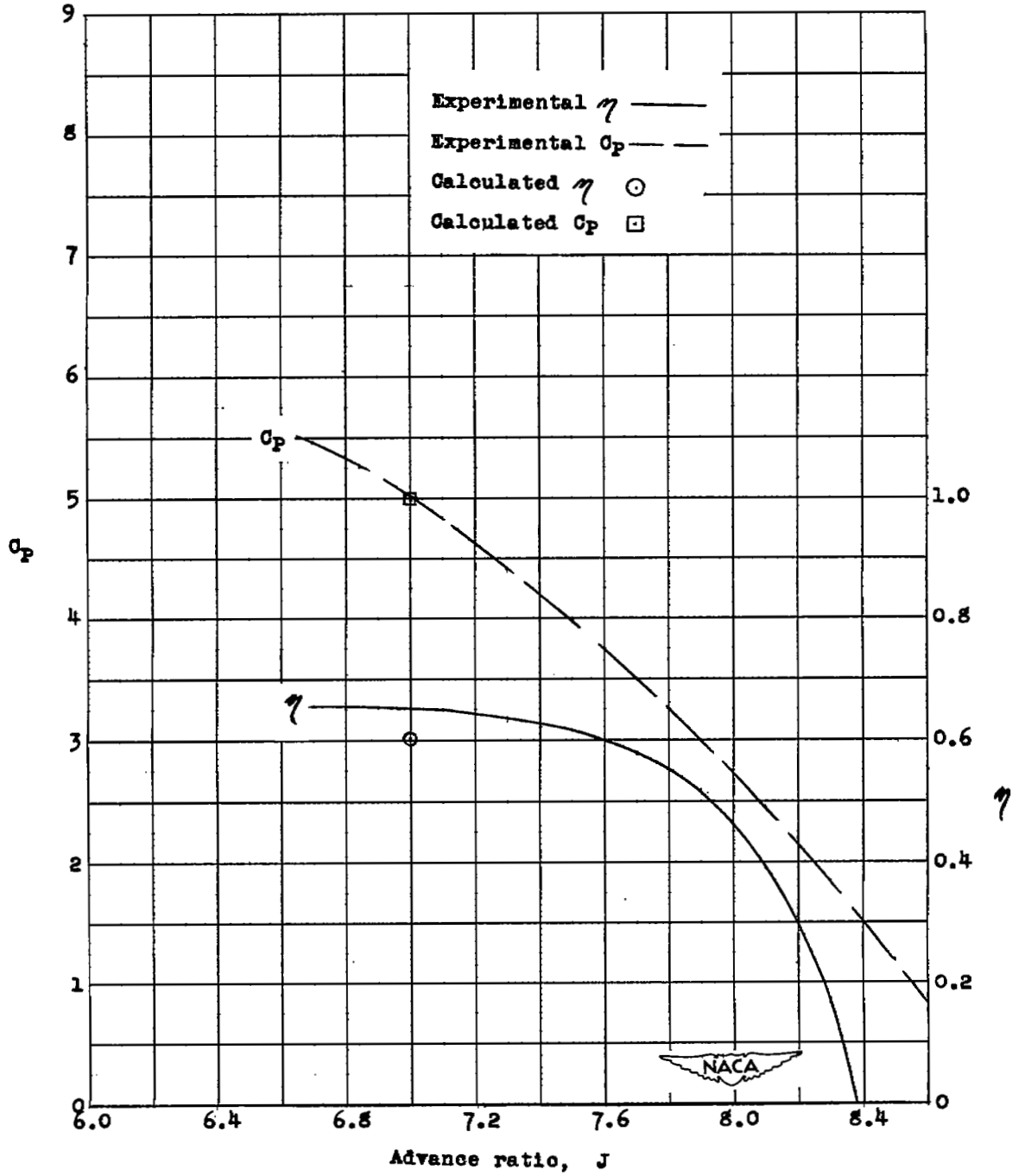

Figure 12.- Comparison of experimental η and C_P with calculated η and C_P. $M = 0.90$; $\beta_F = 75^\circ$; $\beta_R = 73^\circ$.

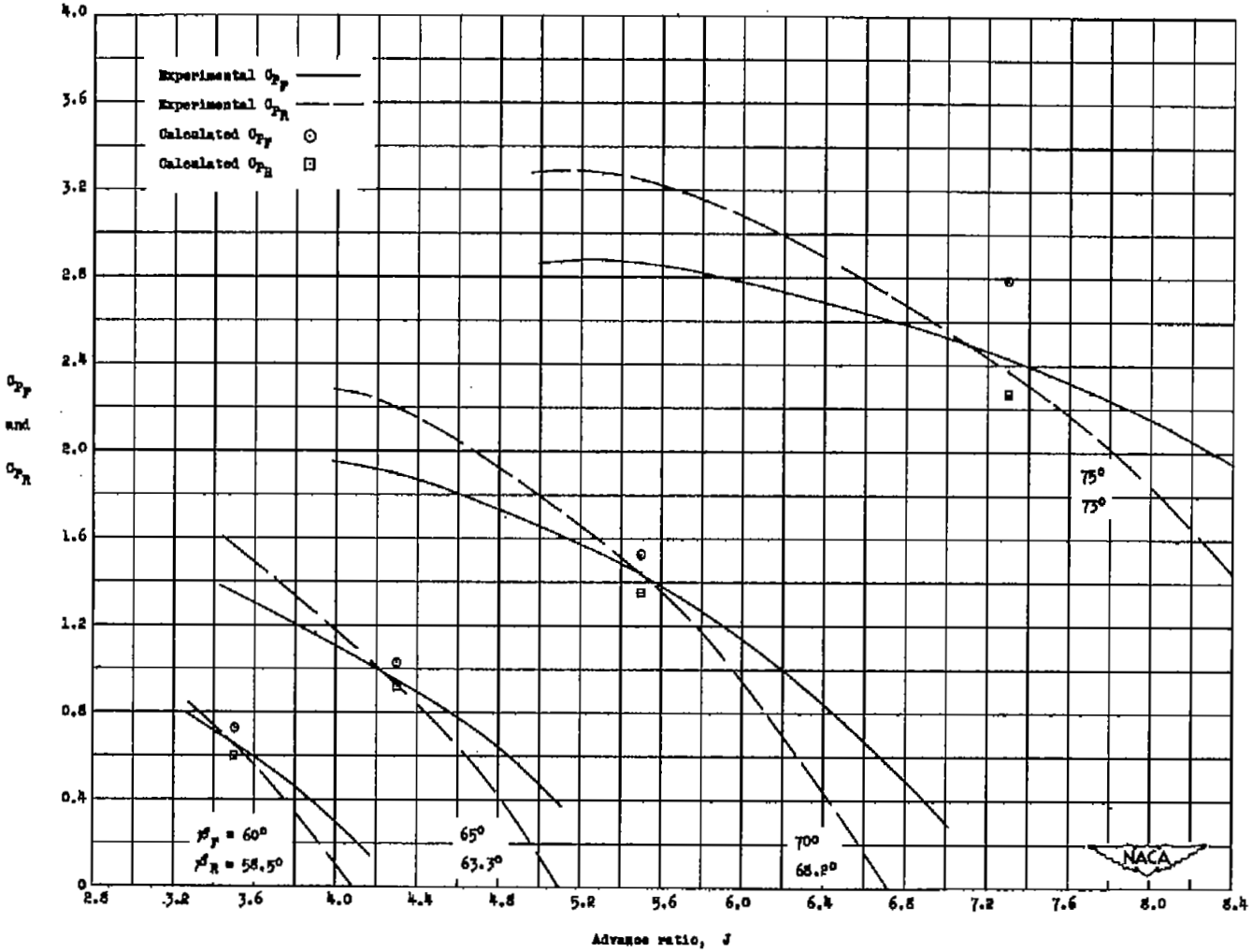

Figure 13.- Comparison of experimental C_{P_F} and C_{P_R} with calculated C_{P_F} and C_{P_R}. M = 0.53.

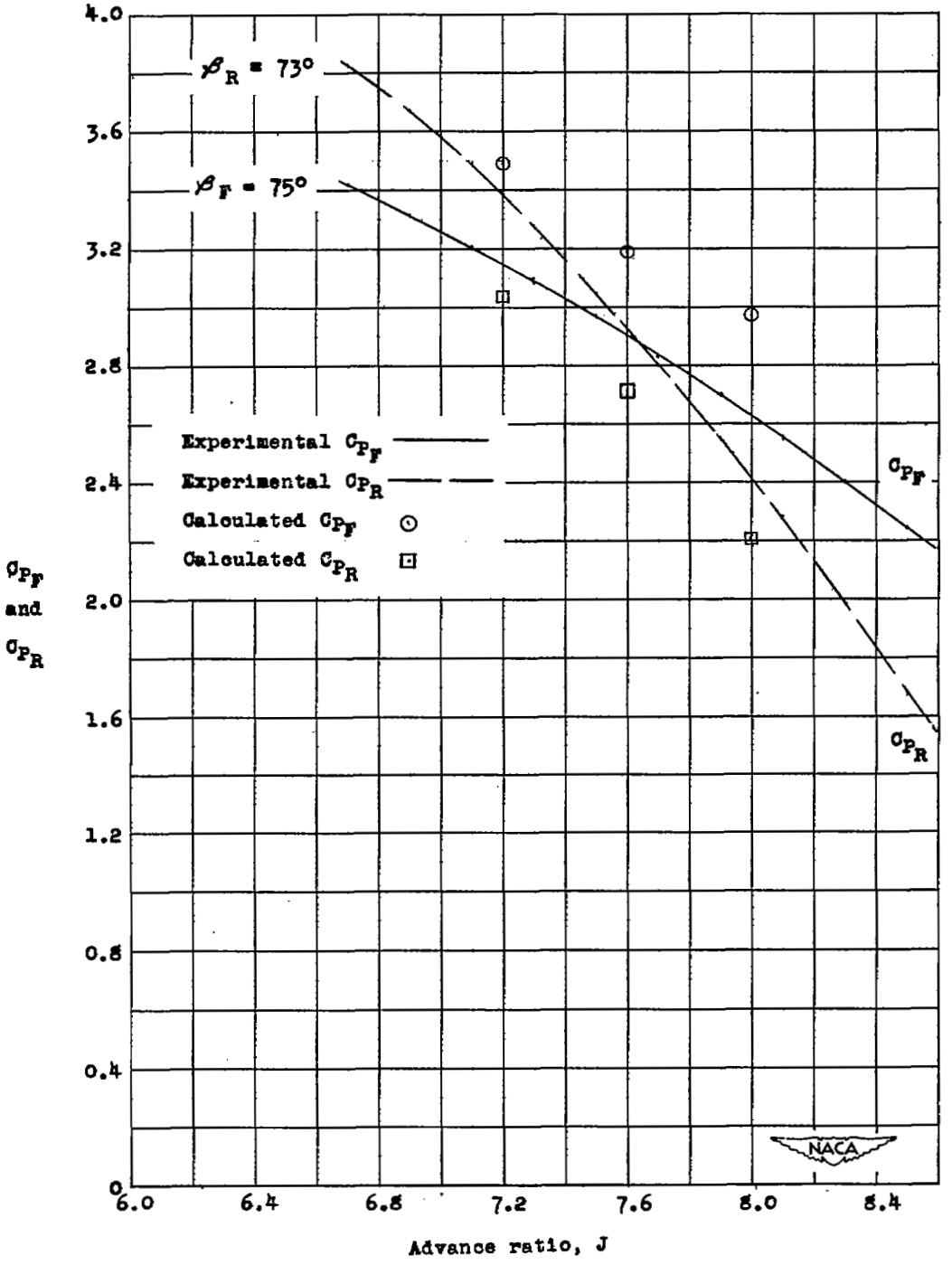

Figure 14.- Comparison of experimental C_{P_F} and C_{P_R} with calculated C_{P_F} and C_{P_R}. M = 0.80; β_F = 75°; β_R = 73°.

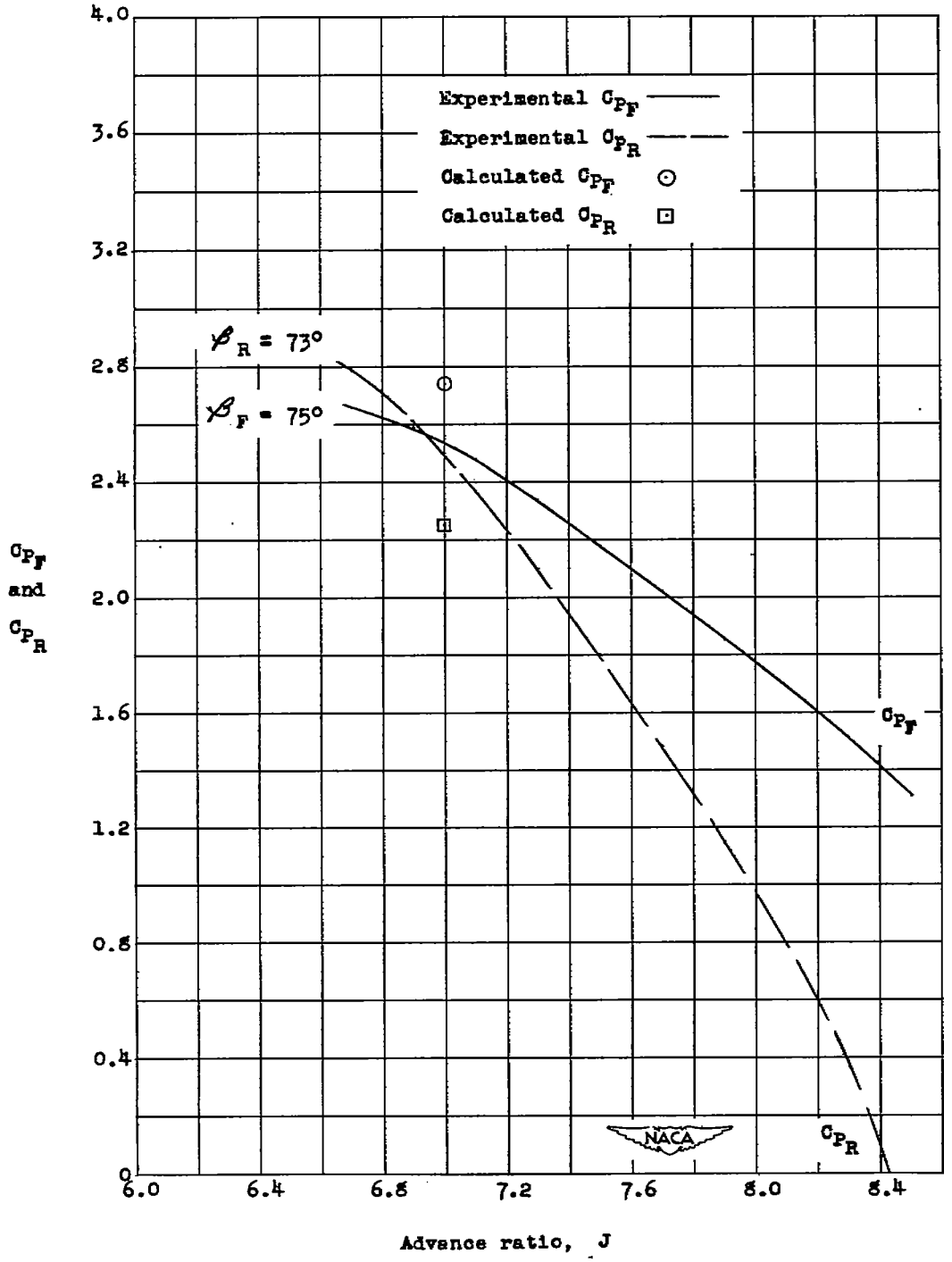

Figure 15.- Comparison of experimental C_{P_F} and C_{P_R} with calculated C_{P_F} and C_{P_R}. M = 0.90; $\beta_F = 75°$; $\beta_R = 73°$.